Synaptotagmin III is a critical factor for the formation of the perinuclear endocytic recycling compartment and determination of secretory granules size

Elena Grimberg[1,2], Ze Peng[1,*], Ilan Hammel[2] and Ronit Sagi-Eisenberg[1,†]

Departments of [1]Cell Biology and Histology and [2]Pathology, Sackler School of Medicine, Tel Aviv University, Tel Aviv, 69978, Israel
*Present address: Laboratory of Molecular Immunology, NHLBI, National Institutes of Health, Bethesda, MD, USA
†Author for correspondence (e-mail: histol3@post.tau.ac.il)

Accepted 24 September 2002
Journal of Cell Science 116, 145-154 © 2003 The Company of Biologists Ltd
doi:10.1242/jcs.00186

Summary

Early endosomes and a perinuclear, Rab-11-positive compartment have been implicated in the recycling of internalized receptors. In this study, we show that synaptotagmin III (Syt III), a member of the Syt family of proteins, is required for the formation and delivery of cargo to the perinuclear endocytic recycling compartment (ERC). We demonstrate that rat basophilic leukemia (RBL-2H3) mast cells endogenously express Syt III, and >70% of this protein colocalizes with early endosomal markers, such as EEA1, annexin II and syntaxin 7, and the remaining protein colocalizes with secretory granule (SG) markers such as β-hexosaminidase, histamine and serotonin. To study the functional role of Syt III, we stably transfected RBL cells with Syt III antisense cDNA and monitored the route of transferrin (Tfn) internalization in cells that displayed substantially reduced (<90%) levels of Syt III (RBL-Syt III$^-$). In these cells, Tfn binding and internalization into early endosomes were unaltered. However, whereas in the mock-transfected cells Tfn was subsequently delivered to the ERC, in the RBL-Syt III$^-$ cells, Tfn remained associated with dispersed peripheral vesicles and Rab 11 remained cytosolic. Nevertheless, the rates of Tfn internalization and recycling were not affected. RBL-Syt III$^-$ cells also displayed enlarged SGs, reminiscent of the SGs present in Chediak-Higashi (beige) mice. However, morphometric analyses suggested that granule formation was unaltered and that the calculated unit granule volume is the same in both cell lines. Therefore, our results implicate Syt III as a critical factor for the generation and delivery of internalized cargo to the perinuclear endocytic recycling compartment and suggest a possible link between ERC and recycling from immature SGs during the process of SG maturation.

Key words: Endocytic recycling compartment, Endocytosis, Synaptotagmin, Transferrin, RBL-2H3 mast cells

Introduction

Synaptotagmins (Syts) constitute a large family of integral membrane proteins implicated in the control of membrane trafficking (reviewed in Adolfsen and Littleton, 2001). Thirteen members of the Syt family have been identified to date. These members display distinct tissue distributions and different Ca^{2+} requirements for binding of syntaxin, phospholipids or homo- and hetero-dimerizations. The best characterized are the neural members Syt I and Syt II, which are synaptic vesicle (SV) proteins that, on the basis of both biochemical and genetic data, have been implicated as Ca^{2+} sensors in the control of neurotransmission (reviewed in Adolfsen and Littleton, 2001). Indeed, knocking out Syt I in mice, mutating the *Syt* gene in *Drosophila* and microinjecting Syt I antibodies into squid giant synapse all resulted in blocking or reduction of the Ca^{2+}-evoked neurotransmitter release (Geppert et al., 1994; Littleton et al., 1994; Mikoshiba et al., 1995). These experiments have therefore validated the role of Syt I as a Ca^{2+} sensor. However, the function of the other members of this family is less understood.

Mast cells are specialized secretory cells that belong to the immune system. Upon activation by either antigen-induced aggregation of their FcεRI receptors or by Ca^{2+} ionophores, these cells release, using a process of regulated exocytosis, a variety of inflammatory mediators, resulting in the immediate allergic reactions (Stevens and Austen, 1989; Galli et al., 1991). We have previously shown that rat basophilic leukemia (RBL-2H3, hereafter referred to as RBL) cells, a mucosal mast cell line, express mRNAs encoding the Syt homologues, Syt II, III and V (Baram et al., 1999). Detailed analysis of the functional role of Syt II, the most abundant homologue in the RBL cells, revealed that Syt II is localized to a late endocytic/lysosomal compartment where it functions to negatively regulate lysosomal exocytosis (reviewed in Baram et al., 2001). We further demonstrated that Syt II is required for the delivery of cargo from the early endosomes to sites of degradation (Peng et al., 2002). In the present study, we set out to investigate the function of Syt III, the second most abundant Syt homologue expressed in the RBL cells. Syt III was previously implicated as a Ca^{2+} sensor of insulin secretion from MIN6 and RINm5F beta cells (Mizuta et al., 1997; Gao et al., 2000). However, in primary islet cells, Syt III was localized to δ cells and more specifically to somatostatin-negative granules (Gut et al., 2001). Finally, in nerve termini the majority of Syt III is expressed in the plasma membrane (Butz et al., 1999). We now demonstrate that in RBL cells, Syt

III is distributed between early endosomes and secretory granules (SGs). We further demonstrate that Syt III is a critical factor for the formation and delivery of internalized cargo from early endosomes to the perinuclear endocytic recycling compartment (ERC). Finally, we show that Syt III and ERC are important factors in the allocation of the SG size.

Materials and Methods

Antibodies

The antibodies used included rabbit polyclonal serum against the cytoplasmic domain of Syt III and monoclonal antibodies directed against the N-terminal region of Syt II (generous gifts from M. Takahashi and Y. Shoji-Kasai, Mitsubishi-Kasei Institute of Life Sciences, Tokyo, Japan), rabbit polyclonal antibodies directed against syntaxin 7 (a generous gift from W. Hong, Institute of Molecular and Cell Biology, Singapore), rabbit polyclonal antibodies directed against $G\alpha i_2$ (AS10, a generous gift from A. Spiegel, The National Institutes of Health, MD, USA), rabbit polyclonal antibodies directed against EEA1 and rabbit polyclonal antibodies directed against Rab11 (generous gifts from M. Zerial, EMBL), monoclonal antibodies directed against annexin II (Transduction Laboratories, Lexington, KY, USA), monoclonal antibodies directed against serotonin (DAKO, Denmark) and monoclonal antibodies directed against T7 (Novagen, Germany).

Reagents

Iron-saturated human Tfn and iron-saturated biotin-labeled Tfn were purchased from Sigma-Aldrich. Fluorescein isothiocyanate (FITC)-conjugated human Tfn was obtained from Molecular Probes (Eugene, OR).

Cell culture

RBL cells were maintained in adherent cultures in DMEM supplemented with 10% FCS in a humidified atmosphere of 5% CO_2 at 37°C.

Cell lysates

RBL cells (10^6) were washed in PBS and resuspended in 30 μl of lysis buffer [50 mM Hepes, pH 7.4, 150 mM NaCl, 10 mM EDTA, 2 mM EGTA, 1% Triton X-100, 0.1% SDS, 50 mM NaF, 10 mM Na PPi, 2 mM $NaVO_4$, 1 mM PMSF and a cocktail of protease inhibitors (Boehringer Mannheim, Germany)] and centrifuged at 12,000 ***g*** for 15 minutes at 4°C. The cleared supernatants were mixed with 5×Laemmli sample buffer to a final concentration of 1×, boiled for 5 minutes and subjected to SDS-polyacrylamide gel electrophoresis (PAGE) and immunoblotting. For the preparation of brain homogenate, whole brain from Wistar rats was homogenized in PBS at 4°C using a Polytron (Kinematica, GmbH, Switzerland, 20 seconds, setting 7). Aliquots (5-10 μg protein) were mixed with 5× Laemmli sample buffer, boiled for 5 minutes and subjected to SDS-PAGE and immunoblotting.

Subcellular fractionation of RBL cells

Cells were fractionated as previously described (Baram et al., 1999). Briefly, RBL cells (7×10^7) were washed with PBS and suspended in homogenization buffer (0.25 M sucrose, 1 mM $MgCl_2$, 800 U/ml DNase I (Sigma-Aldrich), 10 mM HEPES, pH 7.4, 1 mM PMSF and a cocktail of protease inhibitors (Boehringer Mannheim, Germany). Cells were subsequently disrupted by three cycles of freezing and thawing followed by 20 passages through a 21 gauge needle. Unbroken cells and nuclei were removed by sequential filtering through 5 and 2 μm filters (Poretics Co.). The final filtrate was then centrifuged for 10 minutes at 500 ***g*** and the supernatant loaded onto a continuous, 0.45-2.0 M, sucrose gradient (10 ml), which was layered over a 0.3 ml cushion of 70% (wt/wt) sucrose and centrifuged for 18 hours at 100,000 ***g***. Histamine was assayed fluorimetrically after condensation in alkaline medium with O-phthalaldehyde (Shore et al., 1959). The activity of the β-hexosaminidase was determined by incubating aliquots (20 μl) of each fraction (10 μl of sample and 10 μl of 10% Triton X-100) for 90 minutes at 37°C with 50 μl of the substrate solution consisting of 1.3 mg/ml p-nitrophenyl-N-acetyl-β-D-glucosaminide (Sigma-Aldrich) in 0.1 M citrate pH 4.5. The reaction was stopped by the addition of 150 μl of 0.2 M glycine, pH 10.7. The OD was read at 405 nm in an ELISA reader.

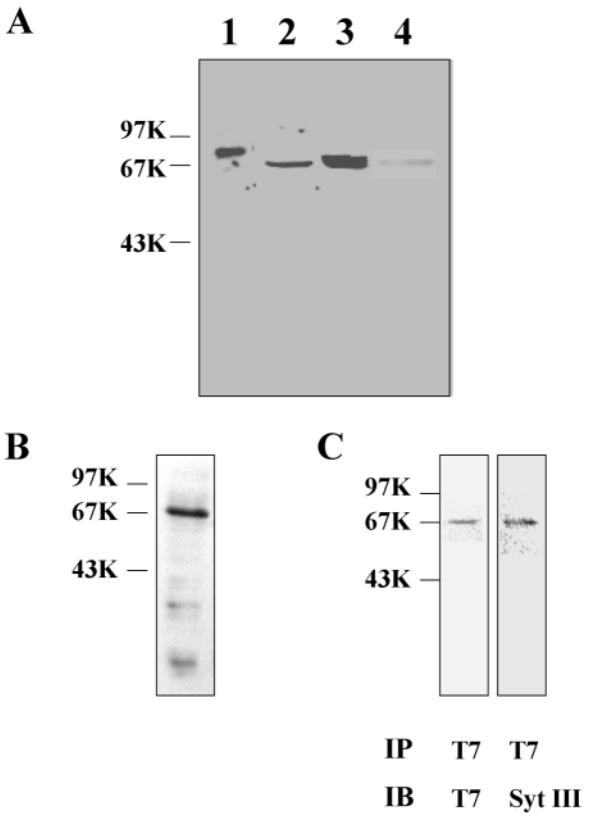

Fig. 1. Expression of Syt III protein in RBL cells and brain. (A) Crude brain homogenate (lane 1, 10 μg protein) and whole cell lysates (1×10^6 cell equivalents) derived from control (lane 2) or Syt III-overexpressing (RBL-Syt III$^+$, lane 3) or Syt III-suppressed (RBL-Syt III$^-$, lane 4) RBL cells were resolved by SDS-PAGE and immunoblotted using a rabbit polyclonal serum directed against the cytoplasmic domain of Syt III (1: 1000 dilution). (B) A whole cell lysate (1×10^6 cell equivalents) derived from RBL cells transiently transfected with T7-tagged Syt III cDNA were resolved by SDS-PAGE and immunoblotted using anti T7 antibodies. (C) Total cell extracts (500 μg) derived from T7-tagged Syt III expressing cells were subjected to immunoprecipitation (IP) using anti T7 antibodies. The immune complexes were resolved by SDS-PAGE and immunoblotted (IB) with either anti T7 antibodies or anti Syt III antibodies, as indicated. Data represent one of three separate experiments.

SDS-PAGE, immunoblotting and immunoprecipitation

Samples were resolved by SDS-PAGE and transferred to nitrocellulose filters. Blots were blocked for 3 hours in TBST (10 mM Tris-HCl, pH 8.0, 150 mM NaCl and 0.05% Tween 20) containing

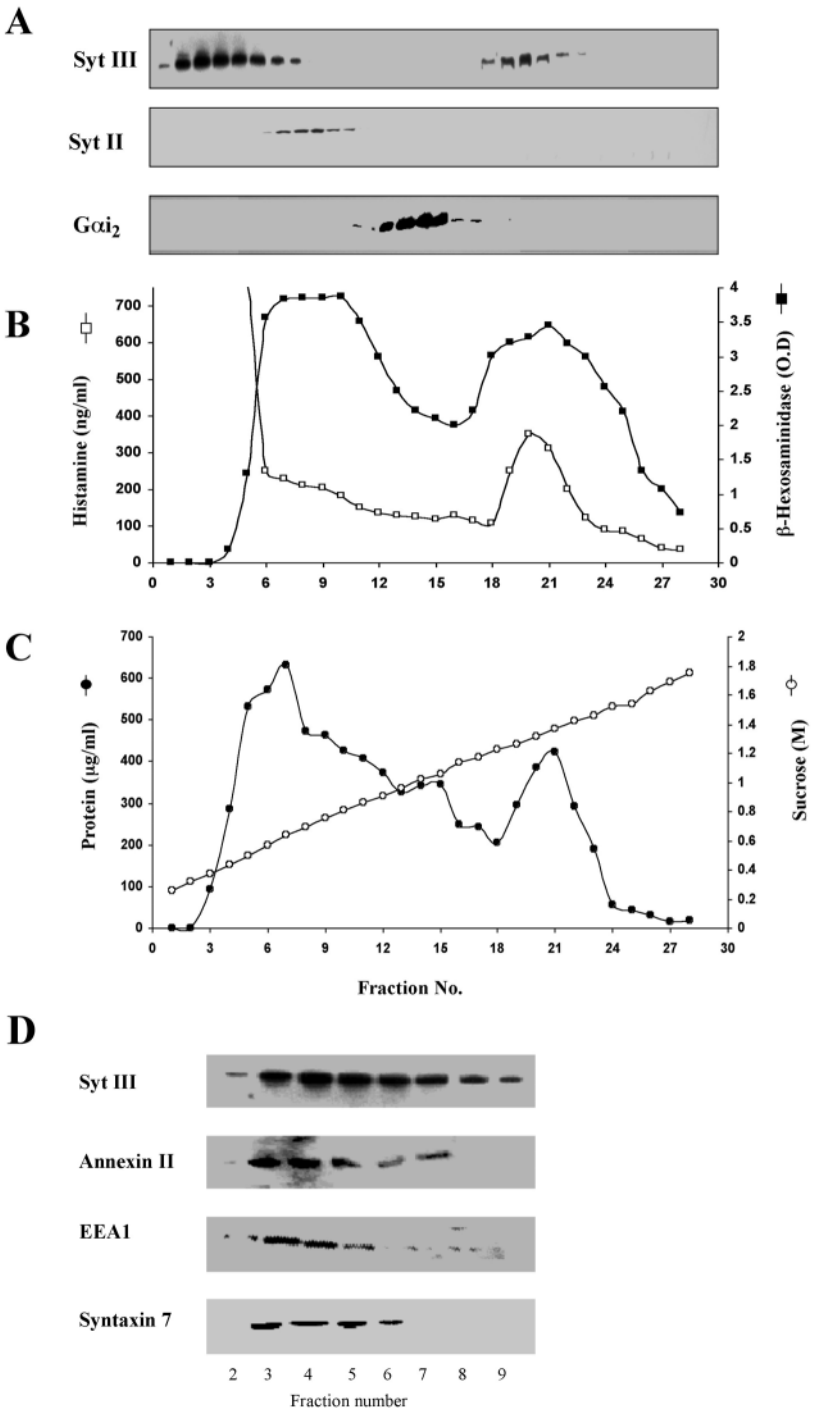

Fig. 2. Subcellular fractionation of RBL cell lysate. Fractions from a continuous sucrose gradient were collected from the top and assayed for (A**)** Syt III (anti Syt III serum 1:1000 dilution), Syt II (monoclonal antibodies 1:1000 dilution) and $G\alpha i_2$ (affinity-purified AS10 antibodies, 1 μg/ml) immunoreactivities. (B) β-hexosaminidase activity (presented as OD read at 405 nm) (■) and histamine content (□). (C) Protein (●) and sucrose density (○). (D) The light density fractions of the gradient were probed for Syt III (polyclonal anti Syt III serum 1: 1000 dilution), Annexin II (monoclonal 1: 5000 dilution), EEA1 (polyclonal anti EEA1 serum 1: 1000 dilution) and syntaxin 7 (polyclonal anti syntaxin 7 antibodies 1: 500 dilution) immunoreactivities. Data represent one of three separate experiments.

5% milk followed by overnight incubation at 4°C with the desired primary antibodies. Blots were washed three times and incubated for 1 hour at room temperature with the secondary antibody (horseradish-peroxidase-conjugated goat anti-rabbit or anti-mouse IgG; Jackson Research Labs). Immunoreactive bands were visualized by enhanced chemiluminescence according to standard procedures. Immunoprecipitation was carried out on cells transiently transfected with T7-tagged Syt III cDNA. Cells were harvested 48 hours after transfection and homogenized in 60 μl of buffer containing 50 mM HEPES, pH 7.4, 250 mM NaCl, 1% Triton X-100, 1mM PMSF and a cocktail of protease inhibitors (Boehringer Mannheim, Germany). After solubilization at 4°C for 15 minutes, supernatants were clarified by centrifugation at 12,000 ***g*** for 15 minutes. Aliquots containing 500 μg protein were incubated for 18 horus at 4°C with anti-T7 tag (1:1000 dilution). Protein A was subsequently added and incubated at 4°C for 1 hour. The beads were collected, washed four times with 50 mM HEPES, pH 7.4, 250 mM NaCl, 0.2% Triton X-100, 1 mM PMSF and a cocktail of protease inhibitors, resuspended in 1×Laemmli sample buffer and boiled for 5 minutes. Immunocomplexes were resolved by SDS-PAGE and subjected to immunoblotting.

Cell transfection

Stable transfection

Full-length rat Syt III cDNA (a generous gift from S. Seino, Chiba University, School of Medicine, Japan) was subcloned into the pcDNA3 expression vector (Invitrogen) in sense or anti-sense orientations. RBL cells (8×10^6) were transfected with 20 μg recombinant or empty vector by electroporation (0.25 V, 960 μF). Cells were immediately replated in tissue culture dishes containing growth medium (supplemented DMEM). G418 (1 mg/ml) was added 24 hours after transfection, and stable transfectants selected within 14 days.

Transient transfection

RBL cells (6×10^7) were transfected with 40 μg of pEF-T7-Syt III cDNA (a generous gift from M. Fukuda, Fukuda Initiative Research Unit, RIKEN, Hirosawa Wako, Saitama, Japan) by electroporation (400V, 960 μF). Cells were immediately replated in tissue culture dishes containing supplemented DMEM.

Immunofluorescence microscopy

RBL cells (2×10^5/ml) were grown on 12 mm round glass coverslips. For immunofluorescence processing, cells were washed twice with PBS and fixed for 30 minutes at room temperature in 3% paraformaldehyde/PBS. Cells were subsequently washed three times with PBSCM (PBS supplemented with 1 mM $CaCl_2$ and 1 mM $MgCl_2$) and permeabilized on ice for 5 minutes with 100 μg/ml digitonin. After two washes with PBSCM, cells were permeabilized for an additional 15 minutes at room temperature with 0.1% saponin in PBSCM. Cells were subsequently incubated for 1 hour at room temperature with the primary antibodies diluted in PBSCM/5% FCS/2% BSA, washed three times in PBSCM/ 0.1% saponin and incubated for 1 hour in the dark with the appropriate secondary antibody (rhodamine- or FITC-conjugated donkey anti-rabbit or anti-mouse IgG, at 1/200 dilution in PBSCM/5% FCS/2% BSA). Coverslips were subsequently washed in PBSCM/0.1%

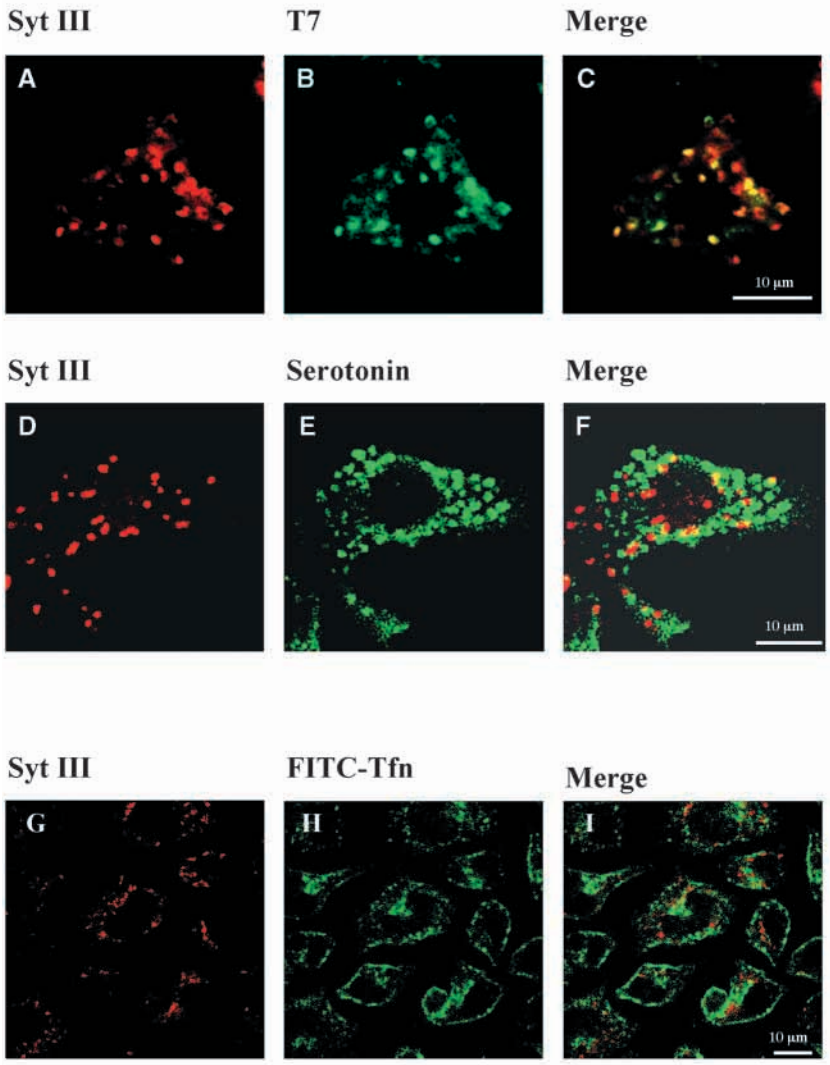

Fig. 3. Localization of Syt III in RBL cells. RBL cells were processed for immunofluorescent staining and visualized by confocal microscopy, as described under Materials and Methods. Cells were incubated with antibodies directed against Syt III (A,D,G, 1:100 dilution), T7 (B, 1:200 dilution), serotonin (E, 1:25 dilution) followed by rhodamine-conjugated donkey anti-rabbit or FITC-conjugated donkey anti-mouse IgG. To monitor internalized Tfn (H), cells were serum starved for 1 hour before incubation for 10 minutes with FITC-conjugated human Tfn (50 μg/ml). Bars represent 10 μm. Data represent one of three separate expreiments.

saponin and mounted with Gel Mount mounting medium (Biomedica corp. Foster city, CA). Samples were analyzed using a Zeiss laser confocal microscope (Oberkochen, Germany).

For colocalization analyses of internalized FITC-Tfn, cells were grown on glass coverslips, serum starved for 1 hour and incubated for the desired time periods with 50 μg/ml FITC-conjugated human Tfn. Cells were subsequently processed for immunofluorescence as described above.

Tfn internalization

RBL cells were plated at 1×10^6 cells/ml and grown for 24 hours. They were subsequently serum starved for 1 hour in DMEM supplemented with 0.2% BSA, followed by a 1 hour incubation at 4°C with biotinylated Tfn (50 μg/ml) to allow binding. Unbound Tfn was removed by washing with ice-cold PBS. To allow endocytosis, the cells were transferred to 37°C for increasing periods of time. The reaction was stopped by placing the cells on ice. To remove surface-bound Tfn, the cells were washed twice with low pH buffer (150 mM NaCl, 50 mM acetic acid, pH 3.5), followed by one wash with ice-cold PBS. Cells were lysed in 100 μl of lysis buffer [50 mM HEPES, pH 7.4, 150 mM NaCl, 10 mM EDTA, 2 mM EGTA, 1% Triton X-100, 0.1% SDS, 50 mM NaF, 10 mM Na PPi, 2 mM $NaVO_4$, 1 mM PMSF and a cocktail of protease inhibitors (Boehringer Mannheim, Germany)], cleared by centrifugation at 12,000 ***g*** for 15 minutes at 4°C and mixed with 5×Laemmli sample buffer. Samples were boiled for 5 minutes and subjected to SDS-PAGE and immunoblotting. Blots were blocked for 1 hour at 4°C in TGG buffer (100 mM NaCl, 50 mM Tris HCl pH 7.4, 1M glucose, 10% glycerol, 0.5% Tween 20) containing 1% milk and 3% BSA, washed once with TGG, twice with TBST at 4°C and finally incubated for 1 hour at 4°C with labeled streptavidin-peroxidase (Sigma-Aldrich) diluted 1:10,000 in TBST. Immunoreactive bands were visualized by enhanced chemiluminescence and quantified by densitometry.

Tfn recycling

RBL cells were plated at 1×10^6 cells/ml and grown for 24 hours. They were subsequently serum starved for 1 hour. Biotinylated Tfn (50 μg/ml) was subsequently added and allowed to internalize for 30 minutes at 37°C. Cells were subsequently transferred to 4°C, and unbound and surface-bound Tfn were removed by washing with cold low pH buffer, followed by two washes with cold medium (DMEM). This procedure resulted in the removal of 95-98% of surface-bound ligand. To measure recycling, cells were warmed to 37°C in the presence of 100 μg/ml of unlabeled Tfn and 100 μM deferoxamine mesylate (Sigma-Aldrich). At selected times, incubations were stopped by placing the dishes on ice and the medium was collected. Cells were washed with ice-cold PBS and lysed in 100 μl of the lysis buffer described above. 40 μl of the collected medium and 10 μl of the cell lysate were subjected to SDS-PAGE, immunoblotting and quantification, as described above.

Electron microscopy and morphometry

RBL cells were harvested, washed once in PBS and fixed with Karnovsky's fixative (Graham and Karnovsky, 1965) for 1 hour at room temperature. They were subsequently washed twice with PBS and postfixed with 1% osmium tetroxide in the same buffer. Dehydration was carried out with graded ethanol and propylene oxide, and tissues were embedded in Araldite. Ultra thin sections (0.075±0.015 μm) were prepared by a LKB III Ultratome, using a diamond knife, and the sections were mounted on Formvar-coated, 200 mesh nickel grids.

Morphometry of granules was performed on randomly obtained electron micrographs (×15,000), as previously described (Hammel et al., 1989). Briefly, organelle cross-sectional areas were measured directly on the transmission electron micrographs. For each experiment, three to five ultra thin sections taken from the two blocks of each group were placed on 200 mesh grids. The section, which was most technically adequate and most clearly stained was selected. Generally, the grid pattern defined two to three complete section windows, the center of which was photographed to provide

prints for granule measurements. Mature granule area (a_i) measurements were carried out on the prints using a graphic tablet (HP 9111A, Hewlett Packard Company, Palo Alto, CA) interfaced to a Power Macintosh 7100/66AV microcomputer for data transformation and analysis. All data were plotted on an HP LaserJet 4000N printer interfaced to the microcomputer. The cross-sectional area (A_i) of each individual granule was converted into the equivalent volume using the simple transformation $v=(4\pi/3)(A_i/\pi)^{3/2}$. The resulting volume equivalents were plotted as a histogram. The multimodal histogram was analyzed by the moving-bin technique to reveal true peaks, as explained elsewhere in detail (Hammel et al., 1983). The periodicity of the distribution was extrapolated as the mean of the intermodal spaces.

Statistical comparison analysis between the cumulative curves was performed using the Kolmogorov-Smirnov test (Sokal and Rohlf, 1995).

Results

Expression and cellular distribution of Syt III in RBL cells

PCR analyses combined with RNase protection assays have previously demonstrated that Syt III was the second most abundant Syt isoform endogenously expressed in RBL cells (Baram et al., 1999). To study the expression of Syt III at the protein level, we used an antibody directed against the cytosolic domain of Syt III to probe an RBL cell lysate by western blot analysis. Consistent with previous results (Butz et al., 1999), this antibody recognized an 80 kDa protein present in rat brain (Fig. 1A, lane 1). The same antibody reacted strongly with a 65 kDa protein expressed in the RBL cells (Fig. 1A, lane 2). That this 65 kDa immunoreactive protein indeed corresponded to Syt III was confirmed by several observations. First, transfection of RBL cells with Syt III cDNA cloned either in the sense or antisense orientations resulted in overexpression or suppression of the same 65 kDa immunoreactive protein, respectively (Fig. 1A, lanes 3 and 4). Secondly, transfection of the RBL cells with a T7-tagged Syt III cDNA resulted in the expression of a 65 kDa T7-tagged protein (Fig. 1B). Finally, the T7-tagged protein immunoprecipitated by anti T7 antibodies could be immunoblotted with the antibodies directed against Syt III (Fig. 1C).

Fractionation of the RBL cells on continuous sucrose gradients revealed that Syt III immunoreactivity was distributed between two densities. Most (70±11%, n=4) of Syt III comigrated with fractions two and seven, at ~0.4M sucrose, whereas the remaining 30% comigrated with fractions 19-22, at ~1.3M sucrose (Fig. 2). The latter fractions also contained histamine and β-hexosaminidase activity (Fig. 2) and therefore include the SGs (Baram et al., 1999).

To identify the light-density compartment, with which Syt III might be associated, several organelle-specific markers were used. These analyses have demonstrated that Syt III immunoreactivity cofractionated with early endosomal markers including annexin II, EEA1 and syntaxin 7 (Fig. 2). Notably, Syt III did not fractionate with Syt II, which comigrates with the first peak of β-hexosaminidase activity (fractions 8-10, Fig. 2), confirming its late endosomal/lysosomal location (Baram et al., 1999), nor did it comigrate with $G\alpha_{i2}$, a marker for the plasma membrane (Fig. 2).

Syt III localization was also examined by confocal microscopy, revealing a granular pattern of stain (Fig. 3A,D,G). Moreover, a similar granular pattern and substantial overlap

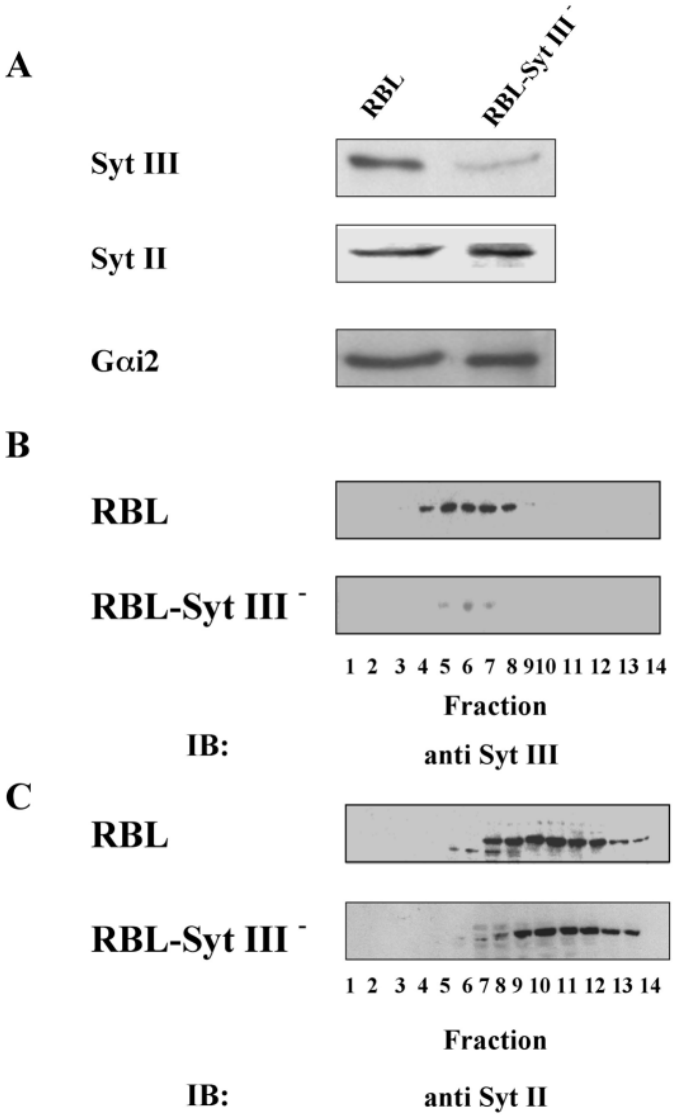

Fig. 4. Suppression of Syt III expression. Whole cell lysates derived from control (empty-vector-transfected) RBL or RBL-Syt III⁻ cells were resolved by SDS-PAGE, immunoblotted and probed (A) with antibodies directed against Syt III (1:1000 dilution), Syt II (1: 1000 dilution) or anti $G\alpha_{i2}$ (affinity-purified AS10 antibodies, 1 μg/ml) as indicated. Sucrose gradient fractions derived from control RBL and RBL-Syt III⁻ cells were resolved by SDS-PAGE, immunoblotted and probed with anti Syt III antibodies (B) or anti Syt II antibodies (C). The first 14 fractions are presented, as indicated. Data represent one of three separate experiments (A) or one of two separate experiments (B,C).

were observed when cells transfected with T7-tagged Syt III cDNA were co-stained with anti T7 and anti Syt III antibodies, confirming the specificity of the antibodies (Fig. 3A-C). However, only a partial overlap could be detected between Syt III and the SG marker serotonin (Fig. 3D-F) or between Syt III and internalized FITC-conjugated transferrin (FITC-Tfn, Fig. 3G-I). In fact colocalization studies with EEA1 revealed a complete overlap between Syt III and EEA1 in a few cells but no overlap at all in others (data not shown). These results therefore suggest that Syt III dynamically cycles to and from the early endosomes.

Suppression of Syt III expression alters the morphology of the recycling compartment in the RBL cells without affecting the rates of Tfn endocytosis or recycling

We have previously shown that transfection of the RBL cells with Syt II antisense cDNA resulted in the specific suppression of Syt II, allowing the assessment of this isoform function (Baram et al., 1999; Peng et al., 2002). Therefore, to study the function of Syt III, we adopted the same approach and stably transfected RBL cells with Syt III antisense cDNA. This transfection reduced specifically the level of Syt III expression without affecting the expression level of other cellular proteins including Syt II and $G\alpha_{i2}$, (Fig. 4A). Fractionation of the RBL-Syt III$^-$ cells on continuous sucrose gradients revealed that the light density endosomal fractions contained significantly reduced amounts of Syt III (Fig. 4B) whereas no Syt III could be detected in the SG-containing fractions (data not shown). By contrast, the amount of Syt II present in the late endosomal/lysosomal fractions remained unaltered (Fig. 4C).

Because Syt III expression in the early endosomal compartment was markedly reduced, in this work we investigated whether receptor-mediated endocytosis was altered in the RBL-Syt III$^-$ cells. To this end we monitored the internalization route of FITC-Tfn in control (empty vector transfected) and RBL-Syt III$^-$ cells.

Following 1 hour of incubation at 4°C, FITC-Tfn was bound to the cell surface of both the control and RBL-Syt III$^-$ cells (Fig. 5Aa,a′). The extent of binding appeared similar in both cell lines indicating that binding to the membranal Tfn receptor was not affected (Fig. 5Aa,a′). To permit endocytosis the cells were warmed up and the uptake of Tfn was monitored. In both the control and the RBL-Syt III$^-$ cells a considerable amount of FITC-Tfn was localized to small vesicles scattered throughout the cytoplasm, after only 1.5 minutes of uptake (Fig. 5Ab,b′). Indeed, monitoring the rate of uptake of biotin-conjugated Tfn indicated similar kinetics of Tfn internalization in both the control and the Syt III suppressed cells (Fig. 5B). These results therefore suggested that Syt III was not required for Tfn internalization.

After 30 minutes of uptake by the control RBL cells, most of FITC-Tfn was found clustered around the cell nucleus (Fig. 6Aa). This perinuclear structure also stained positive for the Rab 11 GTPase (Fig. 6Ab), indicating its correspondence to the endocytic recycling compartment (ERC), a distinct endosomal compartment, responsible for the slow recycling of Tfn (Sheff et al., 1999; Trischler et al., 1999). However, in sharp contrast, following 30 minutes of endocytosis by the RBL-Syt III$^-$ cells, most of the internalized FITC-Tfn remained associated with vesicles scattered throughout the cytosol (Fig. 6Aa′). Furthermore, in these cells, Rab 11 remained mainly cytosolic (Fig. 6Ab′). Hence Syt III appeared essential for the formation of and the delivery of internalized Tfn to the recycling endocytic compartment. Nevertheless, the rate of Tfn recycling, quantified by monitoring the recycling of biotin-conjugated Tfn, was similar in the control and the RBL-Syt III$^-$ cells (Fig. 6B). These results therefore indicated that Syt III and the perinuclear endocytic recycling compartment were not required for Tfn recycling to the plasma membrane.

Alteration of the SG size in RBL-Syt III$^-$ cells

Electron microscopy of RBL-Syt III$^-$ cells revealed the presence

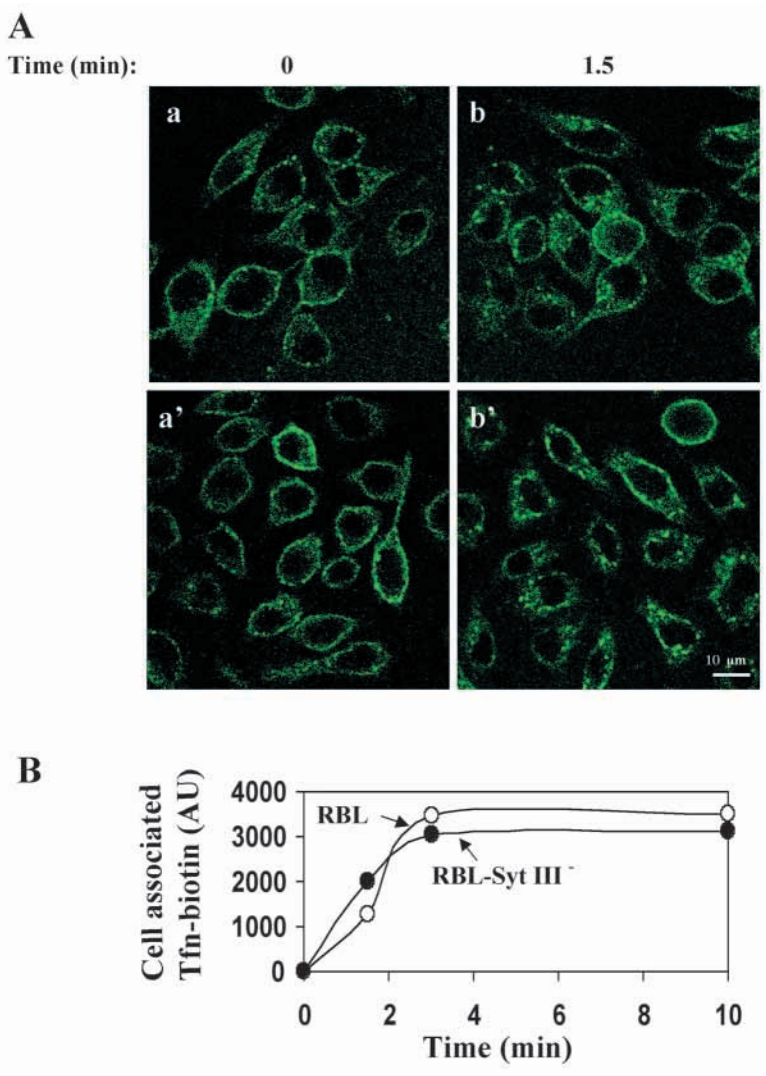

Fig. 5. Internalization of FITC-Tfn in control and RBL-Syt III$^-$ cells. (A) Control RBL (a,b) or RBL-Syt III$^-$ cells (a′,b′) were grown on glass coverslips, serum starved for 1 hour and incubated with FITC-Tfn (50 μg/ml) for 1 hour at 4°C. Unbound FITC-Tfn was removed by washing with ice-cold PBS and the cells were warmed up to 37°C to allow endocytosis. At time 0 (a and a′) and 1.5 minutes (b and b′) the cells were placed on ice and subsequently visualized by confocal microscopy as described under Materials and Methods. Bars represent 10 μm. Data represent one of three separate experiments. (B) Biotin-Tfn was allowed to internalize as described under Materials and Methods. At the end of the indicated time periods, cell-surface Tfn was removed and the amount of intracellular biotin-Tfn was determined by subjecting cell lysates to SDS-PAGE and immunoblotting. Blots were probed with HRP-conjugated streptavidin, visualized by ECL and the intensities of the bands corresponding to biotin-Tfn were quantified by densitometry. The amount of cell-associated biotin-Tfn is presented as arbitrary units. Data represent one of three separate experiments.

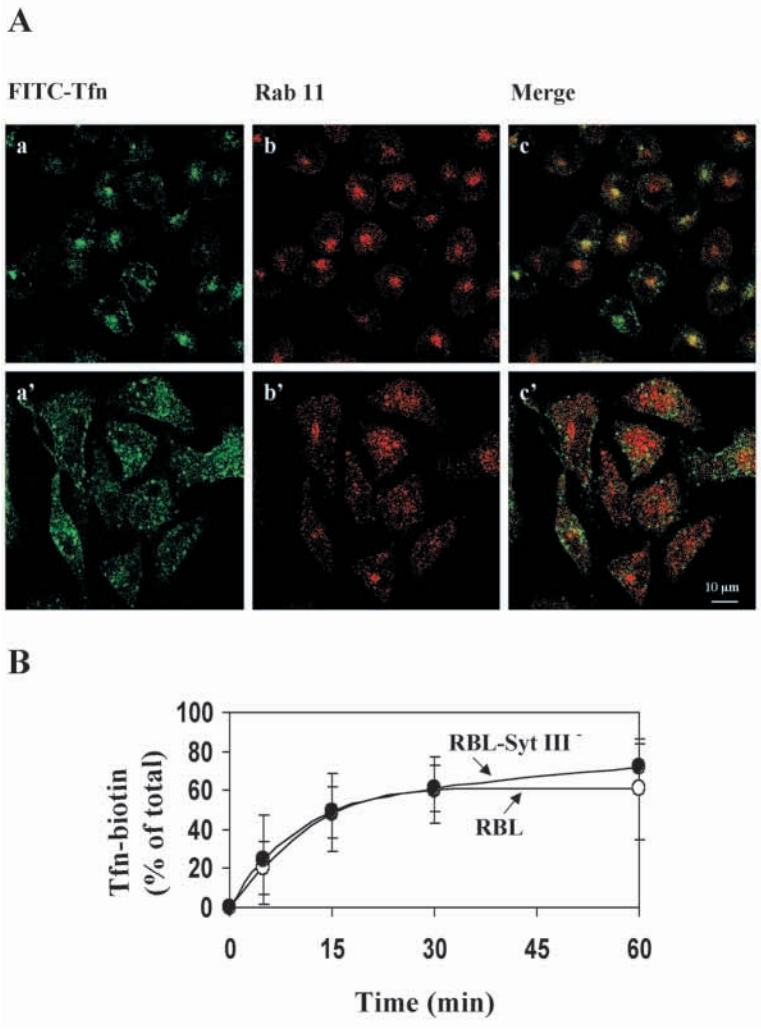

Fig. 6. Recycling of FITC-Tfn in control and RBL-Syt III$^-$ cells. Control RBL (a-c) or RBL-Syt III$^-$ cells (a′-c′) were grown on glass coverslips, serum starved for 1 hour and incubated with FITC-Tfn (50 μg/ml) for 1 hour at 4°C. Unbound FITC-Tfn was removed by washing with ice-cold PBS, and the cells were warmed up to 37°C to allow endocytosis. At the end of 30 minutes, cells were placed on ice and processed for immunofluorescent staining using anti Rab 11 antibodies (polyclonal, 1: 50 dilution). Cells were visualized by confocal microscopy as described under Materials and Methods. Bars, 10 μm. Data represent one of five separate experiments. (B) Tfn recycling was monitored as described in Materials and Methods. The amounts of the extra and intracellular biotin-Tfn were determined by subjecting supernatants and cell lysates to SDS-PAGE and immunoblotting. Blots were probed with HRP-conjugated streptavidin, visualized by ECL, and the intensities of the bands corresponding to biotin-Tfn were quantified by densitometry. The amount of cell-associated biotin-Tfn is presented as a percentage of total biotin-Tfn. The results presented are the average±standard deviations of five independent experiments.

of enlarged SGs in the RBL-Syt III$^-$ cells (Fig. 7A). Granule area histograms demonstrated the size differences quantitatively (Fig. 7B, upper and lower panels). In most (82%) of the control cells, the mean profile area of SGs ranged between 0.4-0.75 μm^2; in 9% of the control cells the average SG size was 0.2 μm^2 and in 9% it was 1.4 μm^2 (Fig. 7B, lower inset). By contrast, in the RBL-Syt III$^-$ cells, in only 60% of the cells the average size of the SGs fell to between 0.4-0.75 μm^2, whereas in 40% of cells, the average size of SGs ranged between 0.9-1.2 μm^2 (Fig. 7B, lower inset). These results therefore indicated that suppression of Syt III resulted in a significantly higher occurrence of enlarged SGs. A moving-bin analysis (Hammel et al., 1988) of the SGs present in both the control and the RBL-Syt III$^-$ demonstrated a similar periodic multi-modal distribution of granules. The value of this mode (indicated by arrowheads, upper inset of Fig. 7B), which corresponds to the volume of a unit granule formed, was calculated from the inter-modal spacing and was found to equal 0.083 μm^3 in both cell lines.

Discussion

We have previously identified Syt III mRNA in the mast cell line RBL-2H3 both by RT-PCR and by RNAase protection assays (Baram et al., 1999). We now provide evidence that RBL cells express Syt III at the protein level, on the basis of its immunoreactivity with specific antibodies (Fig. 1). That the 65 kDa protein recognized by the antibodies used in this study corresponds to Syt III is supported by the following findings. First, transfection of Syt III cDNA into the RBL cells results in the overexpression of the same 65 kDa immunoreactive protein. Second, transfection of Syt III antisense cDNA results in suppression of the same 65 kDa immunoreactive protein. Third, transfection of Syt III T7-tagged cDNA results in the expression of a 65 kDa T7-tagged protein. Finally, the anti Syt III antibodies immunoblot the 65 kDa T7-tagged Syt III protein, immunoprecipitated by anti T7 antibodies. Taken together these results indicate that RBL cells endogenously express Syt III, although its apparent molecular mass in RBL cells is different from that in brain, where it appears as an 80 kDa protein (Butz et al., 1999). Notably, we have previously shown that RBL Syt II has a higher molecular mass (80 kDa) than its brain counterpart, which is 65 kDa (Baram et al., 1999). Therefore, our present and previous results suggest that Syt homologues may undergo cell-specific post-translational modifications. Moreover, these modifications may be linked to the cell-specific location of the Syt homologue and its consequent function. Indeed, fractionation analyses on linear sucrose gradients have indicated that, unlike neurons, where Syt III is located at the presynaptic membrane (Butz et al., 1999), in the RBL cells, approximately 70% of Syt III is associated with early endosomes (EEs), whereas the remaining protein is associated with the SGs (Fig. 2). Whether Syt III is targeted independently to EEs and SGs or whether EEs serve as intermediates in Syt III traffic to the SG is presently unknown. However, previous studies have already demonstrated that cargo internalized by the RBL cells can reach SGs and exocytose in a regulated fashion (Xu et al., 1998). An 80 kDa integral membrane protein of the SG appears at the plasma membrane after exocytosis, from where it is internalized and recycled back to the SG (Bonifacino et al., 1989). Finally, we have recently shown that TPA-induced downregulation of protein kinase Cα (PKCα)

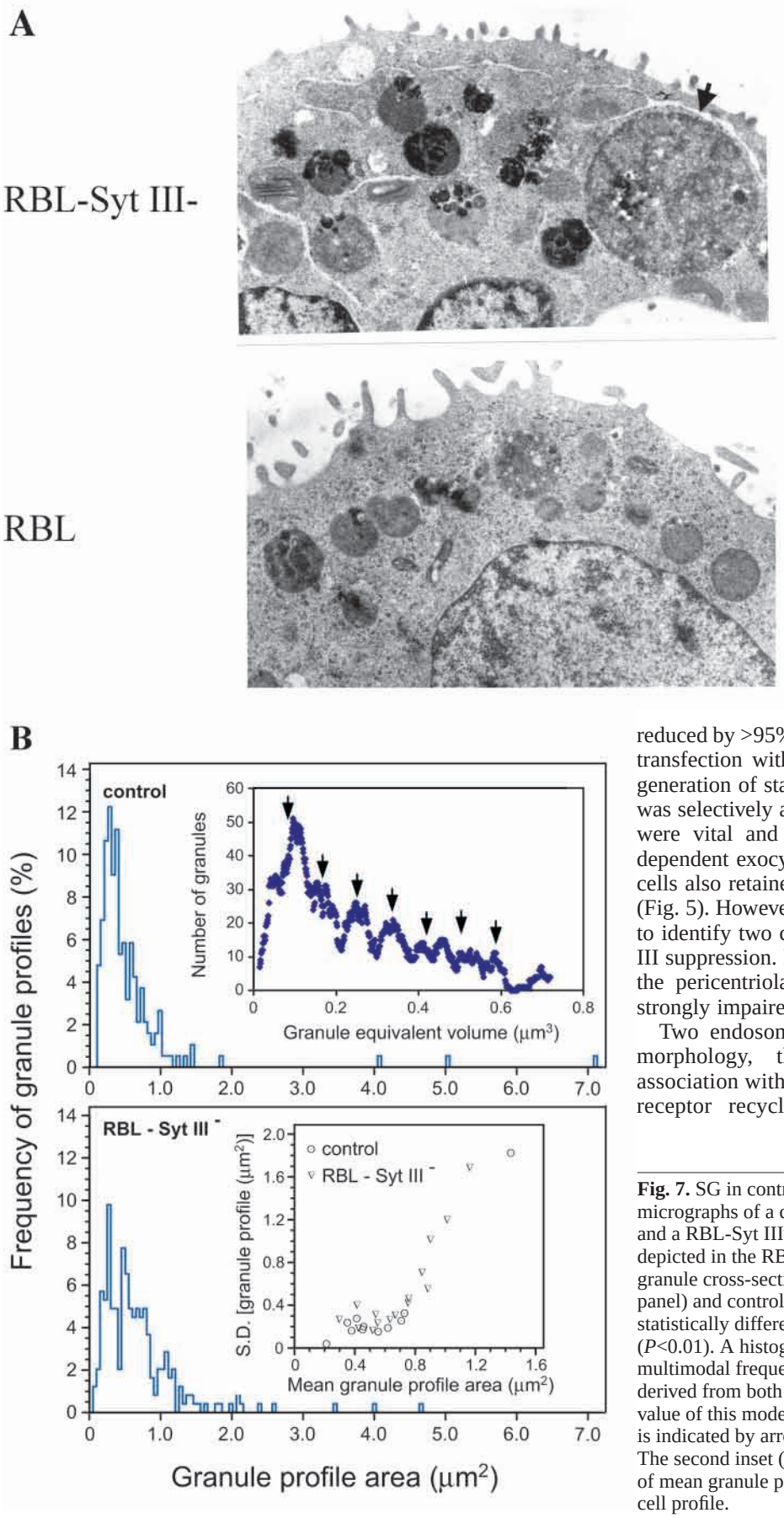

results in trafficking of the enzyme to EEs followed by its appearance on the SG (Peng et al., 2002). These results therefore indicate an intimate connection between endosomes and the SGs. Immunofluorescence analyses confirmed that Syt III is associated with peripheral vesicles (Fig. 3). These vesicles showed, however, only a partial overlap with internalized Tfn (Fig. 3) or the SG marker serotonin (Fig. 3), suggesting that Syt III might be associated with transport vesicles that traffic between these compartments.

In the present study, we focused on the endosome-linked Syt III to explore its possible role in regulating endocytic traffic. To this end, we made use of the RBL-Syt III$^-$ cells, in which the amount of Syt III was specifically and selectively reduced by >90% by transfection with Syt III antisense cDNA (Fig. 4). The antisense approach has proven successful in gaining insight into Syt function in the RBL cells. We have previously demonstrated that stable transfection of RBL cells with Syt II antisense cDNA yielded cell lines in which the level of Syt II was selectively reduced by >95% (Baram et al., 1999). In a similar fashion, transfection with Syt III antisense cDNA resulted in the generation of stable cell lines in which the level of Syt III was selectively and specifically reduced (Fig. 4). The cells were vital and retained their ability to undergo Ca^{2+}-dependent exocytosis (data not shown). The RBL-Syt III$^-$ cells also retained their ability to bind and internalize Tfn (Fig. 5). However, using the antisense approach allowed us to identify two cellular processes strongly affected by Syt III suppression. First, the formation or delivery of cargo to the pericentriolar recycling endocytic compartment was strongly impaired.

Two endosomal compartments, which differ in their morphology, their protein composition and their association with effector proteins have been implicated in receptor recycling. These include the EEs and the

Fig. 7. SG in control and RBL-Syt III$^-$ cells. (A) Electron micrographs of a control (empty vector transfected) RBL cell and a RBL-Syt III$^-$ cell. The arrow points to a 'giant' granule depicted in the RBL-Syt III$^-$ cell. (B) Distribution of measured granule cross-sectional profile areas of RBL-Syt III$^-$ (lower panel) and control cells (upper panel). Both histograms are statistically different based on the Kolmogorov-Smirnov test (P<0.01). A histogram of moving-bin analysis demonstrating multimodal frequency of RBL granule equivalent volumes derived from both cell lines is depicted at the upper inset. The value of this mode is calculated from the inter-modal spacing and is indicated by arrowheads (unit granule volume=0.083 μm^3). The second inset (lower panel) represents a scattergram analysis of mean granule profile area and its standard deviation for each cell profile.

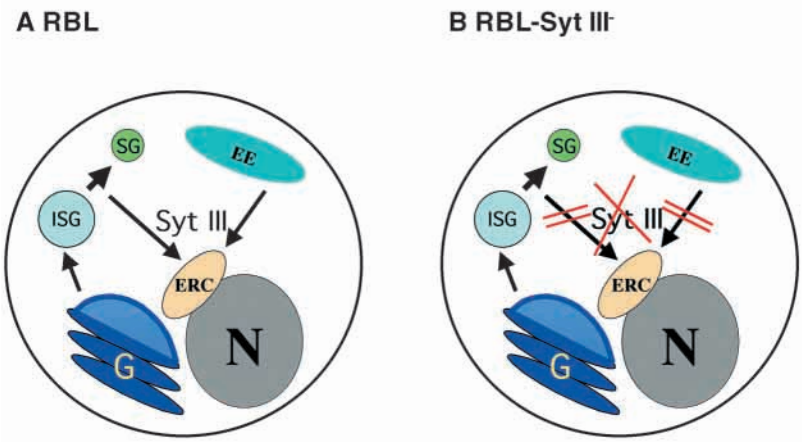

Fig. 8. A model illustrating Syt III function in endosomal trafficking. According to this model, in control cells (A) Syt III regulates the formation of the endocytic recycling compartment (ERC) and the delivery to this compartment from the early endosome (EE) and the immature granule (ISG) during the process of granule maturation. In the RBL-Syt III$^-$ cells (B), suppression of Syt III inhibits the formation of and delivery to ERC from both the EE and the ISG.

pericentriolar endocytic recycling compartment (ERC) that is localized to the vicinity of the nucleus (Sonnichsen et al., 2000). Several proteins have been implicated as playing a role in ERC-dependent traffic. These include the SNARE proteins syntaxin 13 (Prekeris et al., 1998; McBride et al., 1999), syntaxin 6, syntaxin 16, Vti1a, VAMP 3 and VAMP 4 (Mallard et al., 2002) and the Rab GTPases 11 (Ren et al., 1998; Sheff et al., 1999; Trischler et al., 1999) and 6 (Mallard et al., 2002). Another important factor is Rme-1, an EH-containing *C. elegans* homologue (Grant et al., 2001; Lin et al., 2001). However, the molecular mechanism underlying the formation of the recycling endosomes remains obscure. In a recent study, the ERC was clearly demonstrated to form de novo from dynamic structures, which pre-exist in the peripheral cytoplasm (Sheff et al., 2002). Our results strongly support this notion and suggest that Syt III as an essential component in this process. We show that in marked contrast to control RBL cells, in which internalized Tfn is delivered to the Rab-11-positive perinuclear ERC, Tfn is retained in peripheral vesicles in the RBL-Syt III$^-$ cells, whereas Rab 11 remains dispersed in the cytoplasm (Fig. 6). Hence, the reduction in the expression level of Syt III seems not only to impair the delivery of internalized Tfn to the recycling compartment, but it also interferes with its actual de novo formation. Notably, consistent with previous results, the rates of Tfn internalization and recycling remained unaffected in the RBL-Syt III$^-$ cells (Figs 5 and 6). This observation lends further support to previous findings demonstrating that dramatic changes in endosomal morphology have no impact on the kinetics of Tfn endocytosis or recycling (McGraw et al., 1993; Wilcke et al., 2000; Ceresa et al., 2001; Sheff et al., 2002).

The second phenotype observed in the RBL-Syt III$^-$ cells is the significant increase in the number of enlarged SGs (Fig. 7), which is reminiscent of the Chediak-Higashi syndrome, where genetic defects in the LYST gene result in enlarged SGs (Barbosa et al., 1996). Although not proven here, these results indicate a possible connection between the ERC and SG biogenesis (see model, Fig. 8). Indeed, our morphometric analyses suggest that granule formation is unaltered in the RBL-Syt III$^-$ cells (Fig. 7B). On the basis of our calculations, the unit granule volume is the same in both cell types and is about equal (0.083 μm^3) to the unit granule volume in immature mast cells (Hammel et al., 1988). Moreover, the existence of 'giant granules' in both cell lines indicates that the granules undergo homotypic fusion, in a random fashion in both cell lines. Therefore, the increased incidence of 'giant' granules in the RBL-Syt III$^-$ cells most probably reflects a defect in the removal and recycling of proteins from the immature granule (ISG) during the process of granule maturation (see model, Fig. 8). This would imply that the same endocytic compartment that mediates traffic from the EE to the Golgi and plasma membrane mediates SG maturation. Notably, SNAREs are required for the homotypic fusion of ISGs, but their removal is associated with the maturation process (reviewed by Tooze et al., 2001). In fact, in neuroendocrine cells a correlation exists between the removal of Syt IV from ISGs and the acquirement of exocytosis competence (Eaton et al., 2000). Therefore, it will be of interest to investigate whether Syt III fulfills an analogous function in non-neural specialized secretory cells. Another intriguing question regards the possible relationship between Syt III and the LYST protein. LYST has been shown to interact with proteins involved in vesicular transport and is speculated to act as a scaffold for SNARE complex proteins (Tchernev et al., 2002). Our results lend further support to this notion; however, further investigation will be needed to address this question directly.

The molecular mechanism by which Syt III may control ERC formation is presently unknown. The ability of all Syts tested so far to bind to clathrin adaptors as well as SNAREs implies that Syt III may either facilitate coat recruitment and budding of transport vesicles or, alternatively, it may facilitate fusion by interacting with cognate SNAREs. Future studies will be aimed at exploring these possibilities.

We thank L. Mitelman for his invaluable help in all the laser confocal microscopy studies and Dina Amihay for her help in slide preparation for electron microscopy analyses. We thank Y. Zick and D. Neumann for helpful discussions and a critical reading of this manuscript; M. Seino, M. Fukuda, M. Takahashi, Y. Shoji-Kasai, W. Hong, A. Spiegel and M. Zerial for their generous gifts of cDNA and antibodies. Supported by grants from the Israel Science Foundation, founded by the Israel Academy for Sciences and Humanities, by the Israel Ministry of Health (R.S.-E.).

References

Adolfsen, B. and Littleton, J. T. (2001). Genetic and molecular analysis of the synaptotagmin family. *Cell Mol Life Sci.* **58**, 393-402.

Baram, D., Adachi, R., Medalia, O., Tuvim, M., Dickey, B., Mekori, Y. and Sagi-Eisenberg, R. (1999). Synaptotagmin II negatively regulates Ca^{2+}-triggered exocytosis of lysosomes in mast cells. *J. Exp. Med.* **189**, 1649-1658.

Baram, D., Mekori, Y. A. and Sagi-Eisenberg, R. (2001). Synaptotagmin regulates mast cell functions. *Immunol Rev.* **179**, 25-34.

Barbosa, M. D., Nguyen, Q. A., Tchernev, V. T., Ashley, J. A., Detter, J.

C., Blaydes, S. M., Brandt, S. J., Chotai, D., Hodgman, C., Solari, R. C. et al. (1996). Identification of the homologous beige and Chediak-Higashi syndrome genes. *Nature* **382**, 262-265.

Bonifacino, J. S., Yuan, L. and Sandoval, I. V. (1989). Internalization and recycling to serotonin-containing granules of the 80K integral membrane protein exposed on the surface of secreting rat basophilic leukaemia cells. *J. Cell Sci.* **92**, 701-712.

Butz, S., Fernandez, C. R., Schmitz, F., Jahn, R. and Sudhof, T. C. (1999). The subcellular localizations of atypical synaptotagmins III and VI. Synaptotagmin III is enriched in synapses and synaptic plasma membranes but not in synaptic vesicles. *J. Biol. Chem.* **274**, 18290-18296.

Ceresa, B. P., Lotscher, M. and Schmid, S. L. (2001). Receptor and membrane recycling can occur with unaltered efficiency despite dramatic Rab5(q79l)-induced changes in endosome geometry. *J. Biol. Chem.* **276**, 9649-9654.

Eaton, B. A., Haugwitz, M., Lau, D. and Moore, H. P. (2000). Biogenesis of regulated exocytotic carriers in neuroendocrine cells. *J. Neurosci.* **20**, 7334-7344.

Galli, S. J., Gordon, J. R. and Wershil, B. K. (1991). Cytokine production by mast cells and basophils. *Curr. Opin. Immunol.* **3**, 865-872.

Gao, Z., Reavey-Cantwell, J., Young, R. A., Jegier, P. and Wolf, B. A. (2000). Synaptotagmin III/VII isoforms mediate Ca^{2+}-induced insulin secretion in pancreatic islet beta cells. *J. Biol. Chem.* **275**, 36079-36085.

Geppert, M., Archer, B. D. and Sudhof, T. C. (1991). Synaptotagmin II. A novel differentially distributed form of synaptotagmin. *J. Biol. Chem.* **266,** 13548-13552.

Geppert, M., Goda, Y., Hammer, R. E., Li, C., Rosahl, T. W., Stevens, C. F. and Sudhof, T. C. (1994). Synaptotagmin I: a major Ca^{2+} sensor for transmitter release at a central synapse. *Cell* **79**, 717-727.

Graham, R. C. and Karnovsky, M. J. (1965). The histochemical demonstration of monoamine oxidase activity by coupled peroxidatic oxidation. *J. Histochem. Cytochem.* **13**, 604-605.

Grant, B., Zhang, Y., Paupard, M. C., Lin, S. X., Hall, D. H. and Hirsh, D. (2001). Evidence that RME-1, a conserved *C. elegans* EH-domain protein, functions in endocytic recycling. *Nat. Cell Biol.* **3**, 573-579.

Gut, A., Kiraly, C. E., Fukuda, M., Mikoshiba, K., Wollheim, C. B. and Lang, J. (2001). Expression and localisation of synaptotagmin isoforms in endocrine beta-cells: their function in insulin exocytosis. *J. Cell Sci.* **114**, 1709-1716.

Hammel, I., Lagunoff, D., Bauza, M. and Chi, E. (1983). Periodic, multimodal distribution of granule volumes in mast cells. *Cell Tissue Res.* **228**, 51-59.

Hammel, I., Shiloh, R. H. and Nir, I. (1988). Two populations of mast cells on fibroblast monolayers: correlation of quantitative microscopy and functional activity. *J. Cell Sci.* **91**, 13-19.

Hammel, I., Lagunoff, D. and Krüger, P. G. (1989). Recovery of rat mast cells after secretion: a morphometric study. *Exp. Cell Res.* **184**, 518-523.

Lin, S. X., Grant, B., Hirsh, D. and Maxfield, F. R. (2001). Rme-1 regulates the distribution and function of the endocytic recycling compartment in mammalian cells. *Nat. Cell Biol.* **3**, 562-572.

Littleton, J. T., Stern, M., Perin, M. and Bellen, H. J. (1994). Calcium dependence of neurotransmitter release and rate of spontaneous vesicle fusions are altered in *Drosophila* synaptotagmin mutants. *Proc. Natl. Acad. Sci. USA* **91**, 10888-10892.

Mallard, F., Tang, B. L., Galli, T., Tenza, D., Saint-Pol, A., Yue, X., Antony, C., Hong, W., Goud, B. and Johannes, L. (2002). Early/recycling endosomes-to-TGN transport involves two SNARE complexes and a Rab6 isoform. *J. Cell Biol.* **156**, 653-664.

McBride, H. M., Rybin, V., Murphy, C., Giner, A., Teasdale, R. and Zerial, M. (1999). Oligomeric complexes link Rab5 effectors with NSF and drive membrane fusion via interactions between EEA1 and syntaxin 13. *Cell* **98**, 377-386.

McGraw, T. E., Dunn, K. W. and Maxfield, F. R. (1993). Isolation of a temperature-sensitive variant Chinese hamster ovary cell line with a morphologically altered endocytic recycling compartment. *J. Cell. Physiol.* **155**, 579-594.

Mikoshiba, K., Fukuda, M., Moreira, J. E., Lewis, F. M., Sugimori, M., Niinobe, M. and Llinas, R. (1995). Role of the C2A domain of synaptotagmin in transmitter release as determined by specific antibody injection into the squid giant synapse preterminal. *Proc. Natl. Acad. Sci. USA* **92**, 10703-10707.

Mizuta, M., Kurose, T., Miki, T., Shoji, K.Y., Takahashi, M., Seino, S. and Matsukura, S. (1997). Localization and functional role of synaptotagmin III in insulin secretory vesicles in pancreatic beta-cells. *Diabetes* **46**, 2002-2006.

Peng, Z., Grimberg, E. and Sagi-Eisenberg, R. (2002). Suppression of Synaptotagmin II restrains phorbol-ester-induced downregulation of protein kinase Cα by diverting the kinase from a degradative pathway to the recycling endocytic compartment. *J. Cell Sci.* **115**, 3083-3092**.**

Prekeris, R., Klumperman, J., Chen, Y. A. and Scheller, R. H. (1998). Syntaxin 13 mediates cycling of plasma membrane proteins via tubulovesicular recycling endosomes. *J. Cell Biol.* **143**, 957-971.

Ren, M., Xu, G., Zeng, J., de Lemos-Chiarandini, C., Adesnik, M. and Sabatini, D. D. (1998). Hydrolysis of GTP on rab11 is required for the direct delivery of transferrin from the pericentriolar recycling compartment to the cell surface but not from sorting endosomes. *Proc. Natl. Acad. Sci. USA* **95**, 6187-6192.

Sheff, D. R., Daro, E. A., Hull, M. and Mellman, I. (1999). The receptor recycling pathway contains two distinct populations of early endosomes with different sorting functions. *J. Cell Biol.* **145**, 123-139.

Sheff, D., Pelletier, L., O'Connell, C. B., Warren, G. and Mellman, I. (2002). Transferrin receptor recycling in the absence of perinuclear recycling endosomes. *J. Cell Biol.* **156**, 797-804.

Shore, P. A., Burkhalter, A. and Cohn, V. H. (1959). A method for the fluorimetric assay of histamine in tissues. *J. Pharmacol. Exp. Ther.* **127**, 182-185.

Sokal, R. R. and Rohlf, F. J. (1995). In *Biometry: The Principles and Practice of Statistics in Biological Research.* 3rd edn., pp. 571-575. W. H. Freeman Company.

Sonnichsen, B., de Renzis, S., Nielsen, E., Rietdorf, J. and Zerial, M. (2000). Distinct membrane domains on endosomes in the recycling pathway visualized by multicolor imaging of Rab4, Rab5, and Rab11. *J. Cell Biol.* **149**, 901-914.

Stevens, R. L. and Austen, K. F. (1989). Recent advance in the cellular and molecular biology of mast cells. *Immunol. Today* **10**, 381-385.

Tchernev, V. T., Mansfield, T. A., Giot, L., Kumar, A. M., Nandabalan, K., Li, Y., Mishra, V. S., Detter, J. C., Rothberg, J. M., Wallace, M. R., Southwick, F. S. and Kingsmore, S. F. (2002). The Chediak-Higashi protein interacts with SNARE complex and signal transduction proteins. *Mol. Med.* **8**, 56-64.

Tooze, S. A., Martens, G. J. and Huttner, W. B. (2001). Secretory granule biogenesis: rafting to the SNARE. *Trends Cell Biol.* **11**, 116-122.

Trischler, M., Stoorvogel, W. and Ullrich, O. (1999). Biochemical analysis of distinct Rab5- and Rab11-positive endosomes along the transferrin pathway. *J. Cell Sci.* **112**, 4773-4783.

Wilcke, M., Johannes, L., Galli, T., Mayau, V., Goud, B. and Salamero, J. (2000). Rab11 regulates the compartmentalization of early endosomes required for efficient transport from early endosomes to the trans-Golgi network. *J. Cell Biol.* **151**, 1207-1520.

Xu, K., Williams, R. M., Holowka, D. and Baird, B. (1998). Stimulated release of fluorescently labeled IgE fragments that efficiently accumulate in secretory granules after endocytosis in RBL-2H3 mast cells. *J. Cell Sci.* **111**, 2385-2396.